Aerodynamic drag on trains in tunnels Part 2: prediction and validation

A E Vardy, BSc, PhD, FICE, FASCE
Civil Engineering Department, University of Dundee, Scotland

The principal sources of aerodynamic drag on simple trains in tunnels are (a) surface skin friction and (b) stagnation pressure losses at the nose and tail. On sufficiently long trains, the first of these is dominant. On shorter trains, local losses can be more important.

This paper seeks to provide a theoretical basis for predictions of the dependence of drag on the train/tunnel blockage ratio, attention being given to tunnel resistance as well as to train resistance. Hitherto, most predictions have relied on empirical formulae.

It is shown that the train skin friction coefficient varies approximately linearly with the blockage ratio, β_z. The dependence increases with increasing train roughness. The nose loss coefficient k_N is shown to be smaller than 0.1 for reasonably streamlined noses. An approximate relationship between k_N and β_z is hypothesized. The tail loss coefficient k_T is shown to be approximately equal to β_z^2 for poorly streamlined tails. A tail shape *coefficient is introduced for use with more streamlined tails.*

Key words: railway tunnels, high-speed trains, aerodynamic drag, pressure transients, loss coefficients, shape coefficients, train resistance

NOTATION

A	area (m^2)
c	speed of sound (m/s)
C_D	drag coefficient
D	diameter (or equivalent diameter) (m)
f	skin friction coefficient $\equiv \tau_w/(\frac{1}{2}\rho V^2)$
F	force (N)
h	specific enthalpy (J/kg K)
k	stagnation pressure loss coefficient
k_s	characteristic roughness size (m)
l	perimeter length (m)
$\dot{m}$	mass flux $\equiv \rho AV$ (kg/s)
p	static pressure (Pa)
$\mathring{q}$	power per unit length due to external heat (W/m)
Re	Reynolds number $\equiv DV/\nu$
V	velocity (m/s)
$\mathring{w}_s$	power per unit length due to external work (W/m)
β	area blockage ratio $\equiv A/A_t$
Δx	arbitrary length (m)
η	ratio of effective to true areas of train nose
λ	skin friction coefficient $= 4f$
ν	kinematic viscosity (m^2/s)
ξ	tail shape coefficient
ρ	mass density (kg/m^3)
τ	shear stress (Pa)

Superscripts

*	relative to train

Subscripts

ann	annulus
D	drag
F	friction
N	train nose
ref	reference value
s	steady
t	tunnel
T	train tail
u	unsteady
vc	vena contracta
w	wall
z	train (zug)
1–4	specific locations

The MS was received on 16 November 1995 and was accepted for publication on 23 May 1996.

1 INTRODUCTION

The main contributions to overall aerodynamic drag forces on trains in tunnels are well known and their causes have theoretical explanations. Nevertheless, their magnitudes cannot be predicted from theoretical considerations alone. Instead, use has to be made of empirical data obtained from physical measurements. This situation is not ideal, but it is common in engineering practice and appropriate methods of determining the necessary empirical data are well established.

In the absence of the ability to predict values of the various coefficients *ab initio*, the next best possibility would be to use values obtained in some reference condition to predict the behaviour in other conditions. Unfortunately, even this possibility is currently denied to analysts of train drag. No reliable methods exist for the extrapolation of the most important empirical data from one case to another.

The principal purpose of this paper is to provide methods of extrapolating data from one condition to another. A secondary purpose is to examine the likely ranges of values of some key parameters. Where possible, experimental evidence is adduced to provide validation of the proposed theoretical methods. In cases where no experimental data are available, attention is drawn to the tentative nature of the predictions and suggestions are made for filling the gaps. These include physical measurements and three-dimensional numerical simulations.

1.1 Discretization of train/tunnel air flows

Figure 1 is a schematic representation of the conditions in a simple tunnel shortly after train entry. There are five main regions of flow, in each of which the flows

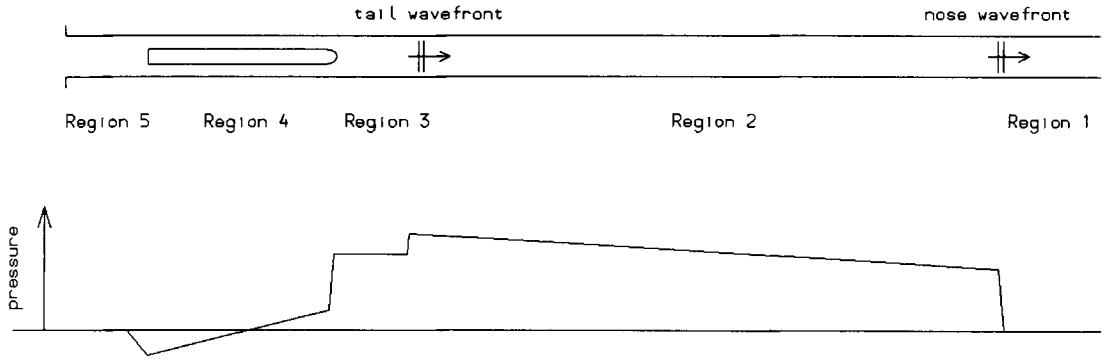

Fig. 1 Pressure distribution shortly after train entry

vary gently. The regions are bounded by

(a) tunnel discontinuities (portals),
(b) train discontinuities (nose and tail),
(c) pressure discontinuities (wavefronts).

All three of these are simplified in Fig. 1, but the figure is adequate for present purposes. If the discontinuities and the regions between them can be simulated accurately, then the complete flow throughout the whole train journey will be predictable. The drag force on the train can then be deduced retrospectively. A major bonus of this approach is that a great deal more can also be deduced retrospectively—pressure histories alongside trains, for example.

The boundaries between regions and the regions themselves are considered in Sections 2 to 6 herein. The emphasis is on the prediction of air flows rather than drag. When the air flows are known, the drag forces can be deduced simply.

1.2 Compressibility

Air flows in railway tunnels are compressible. It is reasonable, however, to neglect the influence of compressibility for many purposes, especially when dealing with phenomena for which necessary empirical data are not known with high accuracy. This approach is adopted in most of the present paper, the only important exception being pressure wavefronts. Elsewhere, compressibility is assumed to be of secondary importance, at least for the purpose of describing stagnation pressure loss coefficients.

A satisfactory global model of transient air flows in tunnel complexes can be developed with these assumptions (that is using acoustic theory). More commonly, account is taken of compressibility, either through a predetermined relationship between pressure and density (**1**) or through a rigorous application of the energy equation (**2**).

2 GEOMETRICAL DISCONTINUITIES—TUNNELS

Figure 2 illustrates the flow through a cross-passage between two tunnels, this being just one of many types of boundary at which the flow parameters change discontinuously from a one-dimensional point of view. There are many other types of boundary and, in each, there are many possible states of flow. The variables include:

(a) different directions of flow,
(b) different rates of flow (Reynolds number dependence),
(c) different *relative* magnitudes of flow in the various limbs of the boundary.

Representative combinations of these variables are considered in texts such as Miller (**3**). Often, it is acceptable to make use of coefficients corresponding to the asymptotic case of high Reynolds number flows.

Local stagnation pressure losses commonly occur in regions of diverging flow. Consider, for instance, the flow through the abrupt change in cross-section shown in Fig. 3. The streamlines cannot cope with the sharp corners and so a region of separated flow exists on the downstream side. One consequence is that the stagnation pressure reduces between the flow sections 1 and 2 and so the (extended) Bernoulli equation is

$$(p_1 + \tfrac{1}{2}\rho V_1^2) - (p_2 + \tfrac{1}{2}\rho V_2^2) = k \times \tfrac{1}{2}\rho V_2^2 \qquad (1)$$

in which p, ρ and V are the air pressure, density and mean velocity respectively and k is a stagnation loss coefficient.

In a few cases, it is possible to predict appropriate numerical values of loss coefficients at tunnel discontinuities using one-dimensional arguments. More generally, it is necessary to resort to experimental mea-

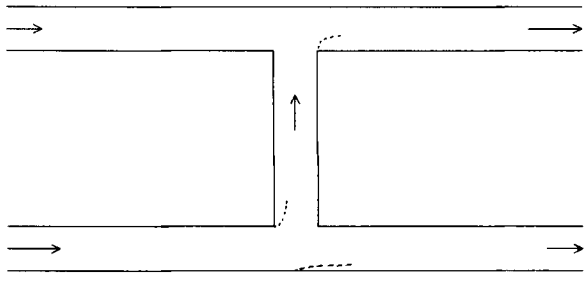

Fig. 2 Typical tunnel boundary (cross-passage)

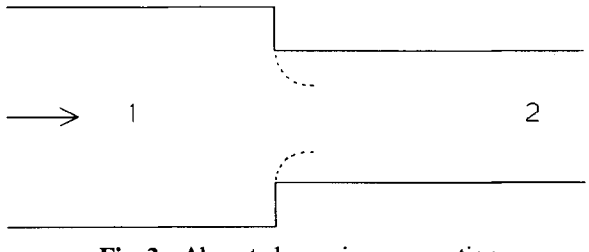

Fig. 3 Abrupt change in cross-section

surements or, if preferred, to three-dimensional flow simulations including suitable turbulence models.

Whichever method is used to obtain the coefficients, the most important characteristic for present purposes is that they may sensibly be regarded as *constants*. Once known, they can be used over and over again in all simulations of train journeys through the particular tunnel, just as equivalent coefficients are used in simulations of other flows in networks—water distribution, for instance. Indeed, the situation in railway tunnels is usually simpler than that in other networks because the Reynolds numbers are so large. It is nearly always acceptable to neglect any dependence of loss coefficients on Reynolds number. In cases where such an assumption is physically unreasonable, the flows are likely to be too small to be of practical interest.

For completeness, it is noted that the numerical values of the loss coefficients can be strongly dependent upon relatively small changes to the local geometry. If the sharp corners in Fig. 3 were replaced by rounded corners, for instance, the lateral extents of the regions of separated flow would reduce. The area available for flow would increase and there would be a smaller loss of stagnation pressure.

The values of the coefficients also depend on the overall geometry. If the area ratio A_2/A_1 in Fig. 3 were closer to unity, the proportional effect of the separated flows would diminish even if their lateral extent remained the same. More likely, their extent would reduce and so there would be two effects causing a reduction in the loss coefficient.

2.1 Quasi-steady flow

Strictly, equation (1) (and most other equations herein) is applicable only to steady flows; the coefficient k is a steady flow loss coefficient that is not exactly applicable in unsteady flows. In practice, however, the flow at any particular location in a tunnel is either steady or slowly varying for most of the time. Rapid changes occur only when wavefronts or train boundaries pass by. At other times, the assumption of quasi-steady conditions will yield reasonable predictions in practical train/tunnel configurations.

It is difficult to assess the short-term consequences of using quasi-steady loss coefficients during periods of highly unsteady flow. It is less difficult, however, to assess medium-term consequences because these *are* determined by the quasi-steady behaviour. In effect, if too much (or too little) change is simulated during a short-lived event, then the subsequent quasi-steady flow will automatically seek to compensate for it.

The theoretical justification for this assertion is straightforward, but lengthy. For present purposes, it is sufficient to note that there is no reported evidence of measurable medium-term errors arising from the assumption of quasi-steady behaviour at geometrical discontinuities in tunnel flows. Nevertheless, some short-lived fluctuations are strongly dependent on the three-dimensional nature of the local flows at discontinuities [see, for example, references (**2**), (**4**) and (**5**)].

3 GEOMETRICAL DISCONTINUITIES—TRAINS

Flows local to train discontinuities may be treated similarly to those at tunnel discontinuities. In this section, relationships are developed between nose and tail loss coefficients and the associated regions of separated flows. The relationships provide approximate methods of extrapolating reference data to non-reference conditions and, in special cases, enable estimates to be made of likely magnitudes of the coefficients. Attention is restricted to the particular cases of flows at the nose and tail. Other train discontinuities—between locomotives and coaches of different size, for instance—could be treated in a broadly similar manner.

The need for these predictive tools is not restricted to trains travelling through more than one tunnel. It also arises with tunnels that have changes in cross-section. The geometrical constraints on the flows are functions of the tunnel as well as the train.

3.1 Train nose

Figure 4 depicts the flow past a flat-fronted train nose. Conditions are shown relative to the train so that it is 'stationary' and the tunnel wall is moving. In principle, the boundary may be either at the front or the rear of the train. The term 'nose' is used to indicate the direction of flow relative to the train, rather than a physical location (for example at the front).

A flow separation is depicted just downstream of the nose and the conditions are closely analogous to those shown in Fig. 3 at an abrupt change in the tunnel cross-section. The extended Bernoulli equation may be written as

$$(p_1 + \tfrac{1}{2}\rho V_1^{*2}) - (p_2 + \tfrac{1}{2}\rho V_2^{*2}) = k_N \times \tfrac{1}{2}\rho V_2^{*2} \qquad (2)$$

in which the asterisk denotes a velocity relative to the train and k_N is the nose loss coefficient.

In the simplest case of a well-streamlined nose, the loss coefficient will be close to zero. The conditions necessary for this are discussed in the following paragraphs. Firstly, however, it is useful to confirm that the coefficient k_N is *not* a property of the train alone. This may be achieved by comparison with Fig. 3. There is ample evidence to show that the loss coefficient for that case is dependent on the area ratio A_2/A_1 [for example see reference (**3**)]. By implication, the same must be true for the analogous situation in Fig. 4, even though the location of the geometrical blockage is different. An approximate method of predicting the nature of this variation is given in Section 3.1.2.

3.1.1 Small nose coefficients

It is easy to show that the nose loss coefficient is very small in many cases. The most reliable way to do so is by reference to experiment, using data such as that

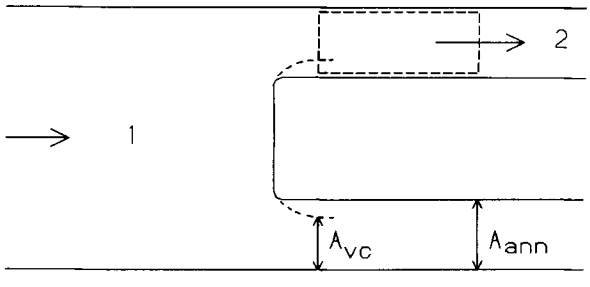

Fig. 4 Separation behind a train nose

obtained by Dayman *et al.* (**6**) at the Jet Propulsion Laboratory in California. Dayman catapulted model trains through a tunnel that could be equipped with a variety of modifications. For present purposes, however, only the simplest tunnel configuration—a straight tube—is considered.

A vital advantage of using Dayman's model data in preference to full-scale measurements of real trains is that there are fewer uncertainties. Most important of all, the cross-sectional areas of the train and the tunnel are known with high precision. Assuming that the train speed and air temperature were measured accurately, the only important unknown in the first few moments after train entry is the nose loss coefficient.

Dayman describes the trains as 'aluminium tubes which were sealed off at each end *with the corners slightly rounded*' (present author's italics). The radius of the slight rounding is not specified, but photographs are provided, showing that the ends of the train are essentially flat fronted. The shape illustrated in Fig. 4 is indicative of the model trains.

The two curves in Fig. 5 show predicted pressure histories at the location of a pressure transducer in the tunnel shortly after train entry, based on nose loss coefficients of $k_N = 0$ and 0.2 respectively. These particular predictions have been made with the computer program AEROTUN, which has been shown by Glöckle and Pfretzschner (**7**) to give good agreement with full-scale measurements, at least for short times. Other programs [for example see reference (**2**)] yield almost identical results so the theoretical approach is well validated.

Dayman's experimental measurements are shown by the symbols +. By inspection, they fall slightly below the $k_N = 0$ line. It is concluded that even flat-nosed trains can have very small loss coefficients in tunnels provided that their edges are sufficiently rounded—although it is noted that real trains are more complex than Dayman's simple models, even close to the train nose. Notwithstanding this reservation, however, the result is physically plausible; as implied in Fig. 4, the smaller the angle of attack at the leading edge of separation, the smaller the lateral extent of any region of separated flow.

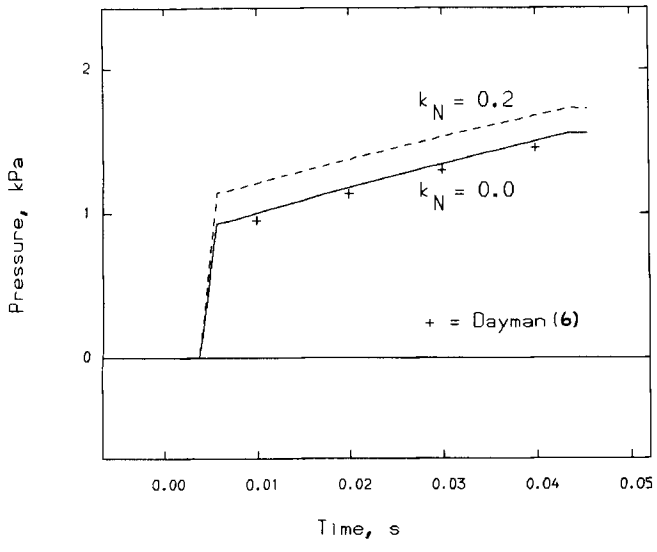

Fig. 5 Influence of nose coefficient on tunnel entry pressures

3.1.2 *Non-zero nose coefficients*

It is possible to obtain some guidance on the likely magnitudes of non-zero nose loss coefficients by estimating the implied width of the separated flow region just downstream of the nose. The continuity, momentum and Bernoulli equations can be written for the flow from the vena contracta (vc) to section 2 in Fig. 4 as

$$\rho A_{vc} V^*_{vc} = \rho A_{ann} V^*_2 \tag{3}$$

$$p_{vc} - p_2 = \rho V^{*}_2 (V^*_2 - V^*_{vc}) \tag{4}$$

$$(p_{vc} + \tfrac{1}{2}\rho V^{*2}_{vc}) - (p_2 + \tfrac{1}{2}\rho V^{*2}_2) = k_N \times \tfrac{1}{2}\rho V^{*2}_2 \tag{5}$$

respectively in which the whole of the nose stagnation pressure loss is assumed to occur downstream of the vena contracta.

By eliminating the pressure difference $(p_{vc} - p_2)$ from equations (4) and (5), it can be shown that the velocities relative to the train at the vena contracta and section 2 satisfy

$$\frac{V^*_{vc}}{V^*_2} = 1 + \sqrt{(k_N)} \tag{6}$$

Using the continuity equation (3), the ratio V^*_{vc}/V^*_2 may alternatively be expressed as A_{ann}/A_{vc} so equation (6) shows that the ratio of the areas of flow at the two locations is equal to $1 + \sqrt{(k_N)}$ or, in terms of blockage ratios,

$$\frac{1 - \beta_z}{1 - \beta_{vc}} = 1 + \sqrt{(k_N)} \tag{7}$$

where β_{vc} denotes the effective blockage ratio (of the train and the separated flow) at the vena contracta.

This relationship is shown in Fig. 6. By inspection, even small values of k_N imply quite large separated flows. For example, a loss coefficient of $k_N = 0.1$ implies an effective reduction of almost 25 per cent in the area of the annulus. It does not seem likely that reasonably streamlined train noses will induce such large separated flows in main-line tunnels. If not, it follows from equation (7) that their nose loss coefficients must be small.

Gaillard (**8**) presented experimental evidence that supports this conclusion. He compared the pressure rises induced by two locomotives entering the same

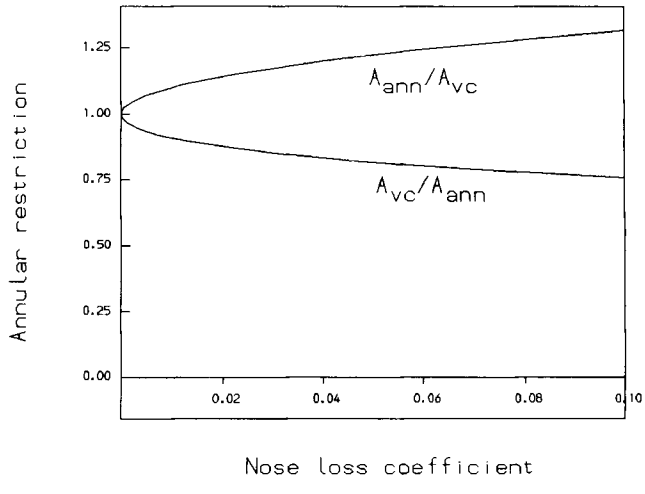

Fig. 6 Blockage implied by nose coefficients

tunnel at the same speed. He observed that they produced the same wave amplitudes, in spite of the more streamlined shape of one of them. He reported that both had the same cross-sectional area and concluded that the magnitude of the nose entry wavefront depends more strongly on the blockage ratio than on the nose shape.

It is not safe to rely too strongly on Gaillard's evidence because the method of defining the area is not specified. Nevertheless, it is reasonable to assume that the same method was used in both cases and hence to accept his assertion that the two areas were nearly equal. It follows that the nose loss coefficients for the two locomotives were also approximately equal.

3.1.3 Variation of nose loss coefficient with blockage ratio

In cases when the nose loss coefficient is not negligible, it is desirable to be able to estimate its dependence on the tunnel area. It is possible to derive a plausible theoretical relationship by postulating an extrapolation of the discussion in the preceding section. Suppose that the nose coefficient k_{NR} is known for one particular blockage ratio β_{zR} (the suffix R denotes reference values). These data may be used to deduce the effective blockage ratio β_{vcR} at the vena contracta for this reference case.

We now introduce a new parameter $\eta \equiv \beta_z/\beta_{vc}$, which is equivalent to the ratio of the true and effective areas of the train. Its value at the reference condition is $\eta_R = \beta_{zR}/\beta_{vcR}$. A second value of η is also known, namely when the train and tunnel areas are equal. In that condition, the true and effective blockage ratios are both equal to unity and so $\eta_1 = 1$.

These two points are highlighted in Fig. 7 and are connected by a straight line which represents a postulated variation of η with β_z. There is no theoretical justification for this particular choice; it is simply the most convenient of all possible choices when no other information is available. In due course, more accurate relationships might be determined from three-dimensional analyses. In the meantime, the postulated linear relationship is more plausible than simply assuming a constant value of k_N.

Provided that reference values are known for k_{NR} and β_{zR} for a particular train, the nose loss coefficient for the same train in a different tunnel can now be estimated as follows:

1. Evaluate β_z for the given train in the given tunnel.
2. Use the relationship depicted in Fig. 7 to deduce the value of η and hence β_{vc}.
3. Use equation (7) to deduce the corresponding value of k_N.

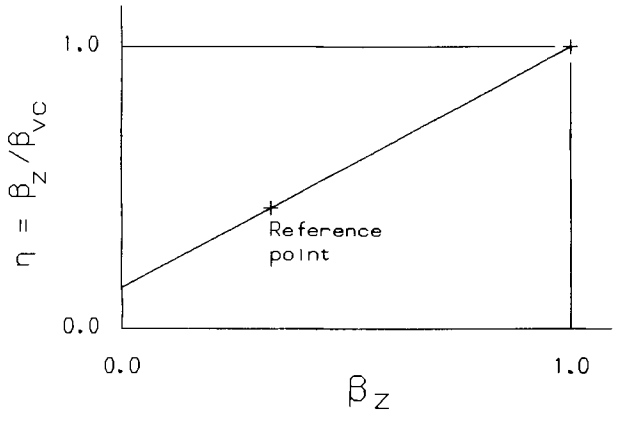

Fig. 7 Postulated influence of blockage ratio

3.2 Train tail

Figure 8 depicts the flow past a flat-faced train tail, conditions being shown relative to the train. A flow separation is depicted just downstream of the tail, enclosing a wake region that can extend for a considerable distance. It is common for the main pressure recovery to occur one or two train diameters downstream of the tail. This complicates the interpretation of experimental data, but it has no particular significance for present purposes.

The extended Bernoulli equation may be written between the flow sections 3 and 4 as

$$(p_3 + \tfrac{1}{2}\rho V_3^{*2}) - (p_4 + \tfrac{1}{2}\rho V_4^{*2}) = k_T \times \tfrac{1}{2}\rho V_3^{*2} \qquad (8)$$

in which k_T is the tail loss coefficient. It is convenient to express the coefficient in terms of V_3^*, not V_4^*, even though the loss in stagnation pressure occurs on the downstream side of the boundary.

If the conditions are regarded as analogous to flow through a sudden expansion, then the magnitude of the loss coefficient can be estimated directly. Firstly, the momentum equation is written between the sections 3A (just behind the tail) and 4 as

$$(p_{3A} - p_4)A_t = \rho(1 - \beta_z)A_t V_{3A}^*(V_4^* - V_{3A}^*) \qquad (9)$$

in which skin friction forces on the tunnel walls are assumed to be negligible.

3.2.1 Abrupt train tails

If Borda–Carnot conditions are assumed to prevail, that is $V_{3A} = V_3$ and $p_{3A} = p_3$, then the pressure difference can be eliminated from equations (8) and (9) to give a simple expression for the tail loss coefficient, namely

$$k_T = \beta_z^2 \qquad (10)$$

The Borda–Carnot condition is a reasonable approximation for many trains. With well-streamlined tails, however, it overestimates the loss coefficient and therefore underestimates the magnitude of the pressure recovery in the wake. With exceptionally poorly streamlined tail shapes, it may underestimate the loss (**6**), but this is an unlikely condition at full scale; that is equation (10) may be regarded as an upper limit for practical purposes.

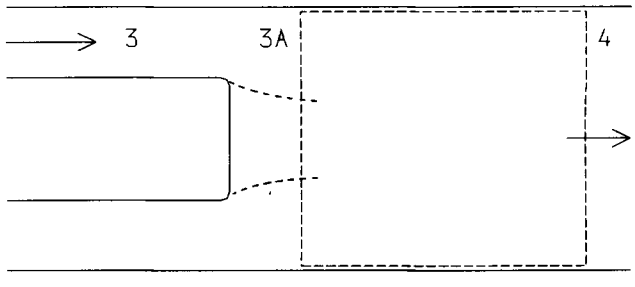

Fig. 8 Separation behind a train tail

3.2.2 Variation of tail loss coefficient with blockage ratio

When Borda–Carnot conditions are a reasonable approximation to the flow past the tail, the variation of the loss coefficient with the blockage ratio is given explicitly by equation (10). At other times, no rigorous method of extrapolating known data is available, but a simple, plausible method is offered in the following paragraphs.

In principle, it would be desirable to develop a method similar to that used for the train nose in Section 3.1.3. In practice, however, it is not possible to define conditions as $\beta_z \to 1$ because the wake will not necessarily fill the tunnel cross-section when the train/tunnel blockage ratio approaches unity. The conditions as $\beta_z \to 0$ are also indeterminate.

A simple, alternative approach is proposed, namely to assume that the tail loss coefficient scales with β_z^2—as is known to be true in the Borda–Carnot case. To achieve this, it is convenient to express the known coefficient at the reference condition as

$$k_T = \xi_T \beta_z^2 \tag{11}$$

and to assume that ξ_T is a constant, independent of the blockage ratio. The constant ξ_T is designated herein as a *tail shape coefficient*.

This method is empirical and it has not been validated, either theoretically or experimentally. Until such evidence can be adduced, the method is justified only on the basis of convenience and/or plausibility. Nevertheless, it should be more accurate than assuming that k_T is constant, independent of the blockage ratio.

4 PRESSURE DISCONTINUITIES—WAVEFRONTS

The only non-geometrical boundaries between regions of continuous flow are pressure wavefronts. Both wavefronts in Fig. 1 are moving in the same direction as the train, but they are of opposite sign; that is the nose wavefront causes an increase in pressure whereas the tail wavefront causes a decrease. Their reflections from the downstream portal or from an intermediate ventilation shaft or cross-passage (Fig. 2) have the opposite signs.

The wavefronts are not created instantaneously. They develop gradually in a three-dimensional manner as the train boundaries pass through the portal region (**5**). As a first-order approximation, a typical nose entry wavefront may be regarded as a linear ramp, beginning when the nose is about $0.75D_t$ in front of the portal and ending about $0.75D_t$ after the portal, where D_t denotes the effective tunnel diameter. The train travels the distance $1.5D_t$ in a time $1.5D_t/V_z$, where V_z denotes its speed, and so the initial length of the ramp is $(c - V_z) \times 1.5D_t/V_z$, where c denotes the local speed of sound. For a train travelling at 250 km/h in a typical tunnel, this distance is of the order of 50 m.

The lengths of the wavefronts change as they propagate along the tunnel. Inertial effects tend to cause steepening of compression wavefronts and elongation of rarefaction wavefronts. Friction tends to cause elongation of both types of wavefront. The inertial behaviour dominates in sufficiently short or smooth tunnels; the friction effect dominates in sufficiently long or rough tunnels.

4.1 Analytical representation

The most suitable theoretical representation of wavefronts in tunnels depends partly upon the purpose of the analysis. It is possible to regard wavefronts either as discontinuous boundaries—as implied in Fig. 1—or as regions of rapidly changing, but continuous, flow. The discontinuous approach is presented here. The continuous approach is more appropriate when numerous wavefronts develop [for example see reference (**1**)].

Figure 9a depicts a wavefront moving at a speed V_w from left to right along a tunnel, changing the velocity of flow from V_1 to V_2. Figure 9b shows the same wavefront at the same instant, but axes are chosen relative to the wavefront—so the tunnel is moving with a speed V_w from right to left. In practice, both $V_1 - V_w$ and $V_2 - V_w$ are negative, so the physical direction of the air flow relative to these axes is opposite to that shown in the figure (mathematically, it is advantageous to use arrows to depict the positive direction of flow).

Relative to the axes used in Fig. 9b, the flow is almost steady. The continuity and momentum equations may be written as

$$\rho_2 A_t(V_2 - V_w) = \rho_1 A_t(V_1 - V_w) \tag{12}$$

and

$$(p_2 - p_1)A_t = \rho_1 A_t(V_1 - V_w)[(V_1 - V_w) - (V_2 - V_w)] \tag{13}$$

The second of these may be expressed in a simpler form by noting that $V_1 - V_w = -c_1$ (that is the local speed of sound). Since the term in square brackets reduces to $V_1 - V_2$, the following equation is obtained:

$$p_2 - p_1 = \rho_1 c_1(V_2 - V_1) \tag{14}$$

4.2 Variation with blockage ratio

Unlike the corresponding relationships at the ends of a train, no empirical coefficient is used in the wavefront

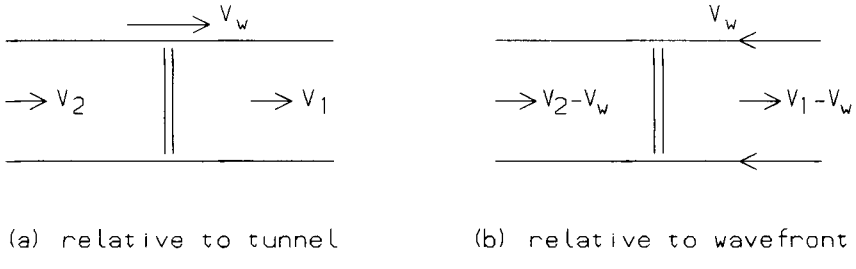

Fig. 9 Propagation of a pressure wavefront

equation (14). Moreover, the equation is independent of the tunnel and train areas. It is valid in the open tunnel and in annular regions alongside trains.

The independence on area is a property of the particular form of the equation. If each velocity were replaced by $\dot{m}/\rho A$, for instance, then a dependence would arise. It is sometimes useful to make such replacements when considering interactions between wavefronts and other contributions to drag.

5 CONTINUOUS FLOW—OPEN TUNNEL

The regions of flow between significant discontinuities subdivide naturally into (a) lengths of open tunnel and (b) annular regions alongside trains. The two cases have much in common, but it is helpful to consider the simpler case first. Additional factors arising in the annular regions are discussed in Section 6.

The continuity, momentum and energy equations may be developed in differential form as

$$\frac{\partial}{\partial t}(\rho A) + \frac{\partial}{\partial x}(\rho A V) = 0 \tag{15}$$

$$\frac{\partial}{\partial x}(pA) + \frac{\partial}{\partial t}(\rho A V) + \frac{\partial}{\partial x}(\rho A V^2) = -\tau_w l_t \tag{16}$$

and

$$-\frac{\partial}{\partial t}(pA) + \rho A\left(\frac{\partial}{\partial t} + V\frac{\partial}{\partial x}\right)(h + \tfrac{1}{2}V^2) = \dot{q} - \dot{w}_s \tag{17}$$

in which τ_w is the wall shear stress, l_t is the tunnel perimeter length, h is the specific enthalpy, $\dot{q}$ is the rate of heat inflow per unit distance and time, and $\dot{w}_s$ is the corresponding rate of work done. For axes chosen relative to the tunnel, $\dot{w}_s$ is zero. For simplicity, the tunnel is assumed herein to be horizontal.

The solution of these equations is outside the scope of this paper. Often, it is acceptable to decouple the energy equation [for example see reference (**9**)]. When this is unacceptable, all three equations must be solved simultaneously, together with additional relationships describing the friction and the rate of heat transfer [for example see references (**2**) and (**10**)].

The key parameter for present purposes is the wall shear stress τ_w, which has a quasi-steady component τ_{ws} and a frequency-dependent component τ_{wu}. The first of these is usually more important and is discussed first. The latter is discussed briefly in Section 5.2.

5.1 Quasi-steady friction

The quasi-steady component of shear stress may be represented adequately by the rough wall relationship (**11**):

$$\sqrt{\left(\frac{1}{4f_t}\right)} = 2\log_{10}\left(\frac{D_t}{k_{st}}\right) + 1.14 \tag{18}$$

in which $f_t \equiv \tau_{ws}/(\frac{1}{2}\rho V^2)$ is a friction coefficient, k_{st} is the characteristic roughness size of the tunnel wall and D_t is the effective diameter of the tunnel. The product $4f_t$ is used instead of f_t in this expression to minimize the likelihood of confusion with an alternative friction coefficient that is sometimes used, namely $\lambda_t \equiv \tau_{ws}/(\frac{1}{8}\rho V^2)$. The relationship between these coefficients is $\lambda_t = 4f_t$.

Strictly, equation (18) is applicable only at high Reynolds numbers, but this is nearly always true in tunnel flows of practical interest. If it is considered necessary to allow for variations in the Reynolds number, use may be made of relationships such as (**12**)

$$\sqrt{\left(\frac{1}{4f_t}\right)} = -2\log_{10}\left(\frac{k_{st}}{3.72D_t} + \frac{5.72}{Re^{0.9}}\right) \tag{19}$$

in which the Reynolds number is $Re \equiv D_t V/\nu$.

If the characteristic roughness size k_{st} could be predicted from purely theoretical arguments, equations (18) or (19) would enable f_t to be deduced explicitly. In practice, however, the characteristic roughness sizes of tunnel walls are not known *a priori*, but must be deduced from past experience. The key distinction between k_{st} and f_t is that the former is representative of the wall surfaces whereas the latter is representative of the whole cross-section.

5.1.1 Variation of tunnel friction with blockage ratio

Suppose that k_{st} can be estimated with sufficient accuracy from experience in other tunnels or from suitable measurements in the particular tunnel under consideration. In this case, the main purpose of equation (18) or (19) will be to predict how the coefficient f_t varies with the effective diameter D_t. This will be useful if the tunnel cross-section is not uniform. It is also useful for the prediction of tunnel wall shear stresses in the annular regions alongside trains.

5.2 Unsteady friction

It is rare for quasi-steady relationships to represent skin friction in tunnels with high accuracy—except during intermediate stages of journeys through long lengths of tunnel between discontinuities (shafts or cross-passages, etc.). When the flows are unsteady, the wall shear stresses are dependent upon accelerations as well as upon mean velocities of flow. Indeed, the wall shear at any particular location depends upon the *historical* conditions at that location as well as upon the instantaneous velocity and acceleration.

Unfortunately, there exists no reliable method of allowing for the unsteady contributions. Researchers have made some progress in understanding the underlying phenomena [for example see references (**13**) to (**15**)], but it is not yet possible to deduce reliable values for the various empirical coefficients. This is an active research area, however, and important advances are expected within a few years.

This is another instance in which three-dimensional turbulent flow analysis could provide valuable data to guide the development and validation of one-dimensional transient analysis. Such analyses could provide detailed predictions of the response of radial velocity profiles to axially moving wavefronts. It is nominally possible to obtain such data experimentally, but the costs of suitable experiments in full-scale tunnels would be high.

6 CONTINUOUS FLOW—TRAIN/TUNNEL ANNULUS

Most of the discussion in Section 5 is also applicable to the annuli around trains. In this case, however, there is a second surface on which shear stresses develop, namely the train. Usually, these stresses are much larger than those on tunnel walls. Indeed, the shear force per unit length on the sides of a train is usually much greater than that on the adjacent tunnel wall, even though the perimeter is smaller.

Two independent factors contribute to the difference. Firstly, the average roughness sizes of train surfaces (including the bogies) are often greater than those of tunnels. Secondly, and much more importantly, the mean velocity of flow relative to a train usually far exceeds that relative to the tunnel. Suppose, for example, that the mean velocity in the annulus is -10 m/s relative to the tunnel and that the train speed is 60 m/s. In this case, $V^2 = 100$ m^2/s^2 whereas $V^{*2} = 4900$ m^2/s^2. The dominance of the latter can be so great that it is reasonable to neglect tunnel wall friction in the annulus, at least in a first-order analysis.

Equations (15), (16) and (17) apply equally to the open tunnel or to an annulus, except for the interpretation of the terms on their right-hand sides. In the momentum equation, the total shear force per unit length is $\tau_{wl} l_t + \tau_{wz} l_z$. In the energy equation, the heat flux per unit length $\mathring{q}$ includes heat from the train as well as heat from the tunnel walls. Finally, the rate of work per unit length $\mathring{w}_s$ is no longer zero. If axes are chosen relative to the tunnel, then work is done by the shear force on the train surface. Alternatively, if axes are chosen relative to the train, then work is done by the shear force on the tunnel surface. If any other axial velocity is chosen for the reference axes, then work is done by the shear forces on both surfaces.

6.1 Quasi-steady friction

The analytical representation of skin friction in an annulus is more complex than that in an open tunnel. Both surfaces contribute to the resistance at any particular flowrate, but their *relative* magnitudes depend upon the flowrate. If it is imagined that boundary layers extend from each surface towards the other, then the lateral position of their 'intersection' varies with the flowrate (**16**). Since the friction coefficients depend upon the nominal boundary layer thicknesses, it follows that they too are dependent upon the flowrate.

Train/tunnel annular flows have been investigated both experimentally and theoretically. In nearly all cases, the cross-sectional geometry has been regarded as two dimensional, either linear or axisymmetric. A simple theoretical approach is outlined by Barrow and Pope (**16**). They assumed the validity of velocity-defect laws in boundary layer regions extending from the train and tunnel surfaces and developed an iterative method of locating a common interface yielding a continuous velocity profile from wall to wall. In that particular paper, it was assumed that one surface is smooth and the other is rough. The methodology is equally applicable, however, to the case of two rough surfaces.

To make use of such methodology, it is necessary to know the characteristic roughness sizes of both the train and the tunnel. Practically, it is necessary to assume that the characteristic roughness size obtained for the tunnel wall in the absence of a train is also valid in the presence of trains. This is not necessarily true, but there is little alternative but to make the assumption. Thereafter, the train wall roughness can notionally be deduced from experimental measurements of flow in the annulus.

In practice, it is most unlikely that any attempt to deduce the train roughness from direct measurements of flow in the annulus will be successful. There is far too much opportunity for error. In particular, it is very difficult to measure the mean flowrate with good accuracy. It can also be difficult to measure the pressure gradient in the annulus and, even if it were measured precisely, the proportions due to friction and acceleration could not be separated with certainty.

Realistically, the estimation of train roughness is best made indirectly, by inference from measurements in other locations. Appropriate methods can be based on the work of, for example, Hara (**17**), Gawthorpe *et al.* (**18**) or Maeda *et al.* (**19**).

6.1.1 *Variation of annulus friction with speed and blockage ratio*

When the characteristic roughness sizes of the train and tunnel surfaces are known, the skin friction forces can be estimated on the two surfaces (a) with alternative mean velocities of flow, (b) with alternative train speeds and (c) in sections of tunnel with alternative effective diameters. For greatest accuracy, a fresh analysis such as Barrow and Pope's (**16**) should be carried out whenever there is any change in any of the above parameters. In practice, however, this would be very time consuming. An alternative, simpler approach is to use their analysis to obtain the roughness sizes k_{st} and k_{sz} and then to use modified versions of expressions such as equation (18) for each surface independent of the other.

As a numerical example, suppose that three different trains have identical cross-sectional areas and perimeters ($A_z = 10$ m^2 and $l_z = 12$ m) but different characteristic roughness sizes ($k_{sz} = 1$, 5 and 20 mm). The implied skin friction coefficients satisfying

$$\sqrt{\left(\frac{1}{4f_z}\right)} \approx 2 \log_{10}\left[\frac{4(A_t - A_z)}{k_{sz}(l_t + l_z)}\right] + 1.14 \qquad (20)$$

are shown in Fig. 10 for a range of blockage ratios.

In all three cases, the predicted dependence of f_z on β_z is almost linear for a wide range of β_z satisfying:

$$\text{When } k_{sz} = 1 \text{ mm}: \quad f_z \approx 0.00290(1 + 1.17\beta_z) \qquad (21)$$

$$\text{When } k_{sz} = 5 \text{ mm}: \quad f_z \approx 0.00400(1 + 1.50\beta_z) \qquad (22)$$

$$\text{When } k_{sz} = 20 \text{ mm}: \quad f_z \approx 0.00535(1 + 2.08\beta_z) \qquad (23)$$

The general form of these relationships is identical to that deduced by Gaillard (**20**) from full-scale measurements (see Section 6.1.2). This suggests that the simple method used to deduce the relationship is reasonable. In particular, it may be expected to be more accurate than simply assuming that the skin friction coefficient is independent of the blockage ratio.

6.1.2 *Empirical relationships between f_z and β_z*

Gaillard (**20**) presented an empirical relationship between train friction coefficients and the blockage

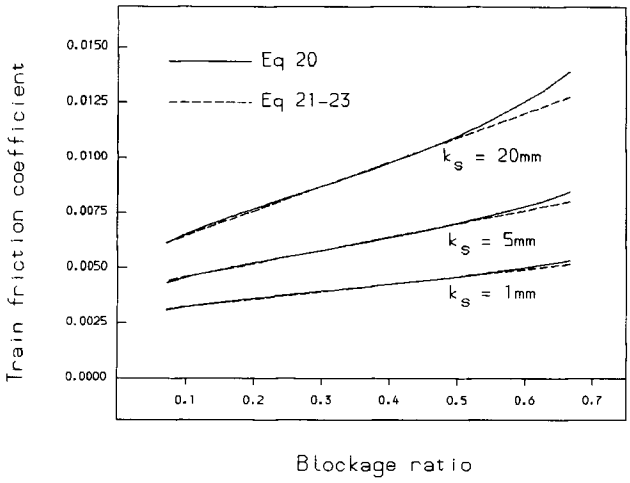

Fig. 10 Influence of blockage ratio on train friction

ratio, namely

$$f_z \approx f_{z0}(1 + 2.21\beta_z) \tag{24}$$

where f_z and f_{z0} denote the train skin friction coefficients in the tunnel and the open air respectively.

This relationship has been used quite widely in practice despite being deduced from a relatively small number of full-scale tests. In the light of the above discussion, however, it seems likely that the coefficient 2.21 is not representative of modern high-speed trains. It might even be an overestimate for the particular trains used in the test programme.

Gaillard's methodology had a number of limitations, including:

1. The number of samples (four) is small.
2. The train area used in the evaluation of β_z is unclear.
3. The skin friction force was necessarily obtained by a process of subtraction involving uncertainties.
4. The velocity used to deduce f_z from the 'measured' skin friction force was itself deduced in an approximate manner.

These comments do not imply laxity in the experimental method. They simply highlight difficulties associated with methods used before wave analyses reached an advanced state. When drag is determined from full-scale measurements today, a completely different methodology should be adopted, based on the coefficients discussed herein.

Equivalent tests with smoother trains were undertaken by Hara (**17**) on the Shinkansen line. Hara deduced friction coefficients from measurements obtained with the same train in various tunnels giving blockage ratios from 0.16 to 0.595. The coefficients tended to be larger in the higher blockage cases, but the results exhibit considerable scatter. Because of this, it is not possible to deduce a reliable expression in the form of equations (21) to (24). Nevertheless, by taking ratios of sample data, it can be shown that the coefficient of β_z is probably towards the lower end of the range given in these equations.

There is undoubtedly a need for further full-scale measurements designed to reduce the level of uncertainty implicit in the above discussion. In the meantime, it seems reasonable to make use of equation (20), either directly or through derived expressions such as equations (21) to (23).

6.2 Unsteady friction

The magnitudes of *unsteady* contributions to the shear stress in the annulus will be comparable to those in the open tunnel. In contrast with that case, however, their importance is relatively small, because the quasi-steady contributions are so much larger. The current inability to predict their magnitudes reliably is not a serious limitation in the annulus. Unsteady friction is not expected to modify conclusions reached in Section 6.1.

7 OVERALL AERODYNAMIC DRAG

Although the purpose of this paper is to advance the state of the art in the prediction of the *overall* aerodynamic drag, attention has focused on individual components of drag, not on the whole. The focusing is not merely convenient; it is *necessary*. Air flows in tunnels are often highly unsteady and the various components of drag do not share a common scaling law. The historical notion of an overall balance between train drag and tunnel drag is valid in principle, but it is rarely usable in practice.

Aerodynamic simulations can provide high-quality, detailed predictions of pressure histories and velocity histories in tunnels provided that adequate empirical coefficients are specified [for example see reference (**7**)]. It is axiomatic that the same simulations must represent the train drag satisfactorily because that is what causes the air flows. The accuracy of the drag predictions therefore depends on little more than the accuracy of the empirical data that must be supplied for the reference cases utilized above.

7.1 Accuracy of empirical data

The data required by typical computer programs define, for the trains and the tunnels:

(a) the geometry,
(b) local stagnation pressure loss coefficients,
(c) skin friction coefficients.

It is usually possible to specify most of the geometrical parameters with good accuracy. The only important exception is the train cross-sectional area or, more precisely, its effective aerodynamic area. It is not sufficient to use arbitrary definitions of train area that have been developed for other purposes [see reference (**21**)].

The values of local stagnation pressure loss coefficients are well documented for most tunnel boundaries. The values for trains are less certain, but the methods presented herein should reduce the uncertainty. The evidence presented in Section 3.1.1 suggests that nose loss coefficients of modern high-speed trains will not exceed 0.1. Likewise, their tail shape coefficients will be smaller than unity (Section 3.2.2).

The principal uncertainties in the empirical data are the skin friction coefficients. The general methodology established over many decades for the evaluation of friction coefficients in pipes and channels applies equally to tunnels, and it is sufficient for many existing ones. Difficulties arise, however, when it is necessary to predict

coefficients for tunnels not yet built, especially when large amounts of equipment and cable, etc., are to be installed on the walls. It can be difficult to find past examples on which to base a judgement. In such cases, estimates of tunnel friction coefficients can easily be in error by more than 20 per cent, perhaps much more. This is unimportant in short tunnels (because inertia forces are the dominant form of tunnel resistance), but it is significant in longer tunnels—where train drag has greatest economic significance.

The estimation of train skin friction coefficients is an even more uncertain process. Modern, high-speed, smooth-walled trains have quite small coefficients ($f_z \leqslant 0.004$, say), but their lengths are much greater than was usual for passenger trains in the past. Their overall aerodynamic drag is strongly dependent on f_z.

7.2 Measurement of train drag coefficients

One important purpose of this paper has been to demonstrate how accurate data for one reference case can be extrapolated to other cases. This is an important capability, but it implies the existence of suitable reference data. Moreover, the reference case must be as accurate as possible because extrapolation techniques have a nasty habit of amplifying errors.

By far the most useful reference data are full-scale measurements—provided that they are accurate and complete. It is undoubtedly possible to obtain such data, but it is most important that the right measurements are taken and that the train and tunnel are well chosen.

8 CONCLUSIONS

1. The most important uncertainty in the estimation of aerodynamic drag on a train in a tunnel is the train friction coefficient. Most other coefficients are either (a) relatively unimportant or (b) capable of being estimated with reasonable accuracy.
2. Measurements at full scale suggest that train friction coefficients increase with the blockage ratio and that the rate of increase is greater with rough trains than with smooth trains.
3. A simple method of reproducing this behaviour has been presented using standard pipe friction relationships. The method reproduces observed experimental behaviour within the limits of accuracy of the reported data. There is an urgent need for more accurate data using modern trains and modern experimental methods.
4. The nose loss coefficients of reasonably streamlined trains will rarely exceed 0.1 and may often be close to zero. A plausible method of predicting the dependence of nose coefficients on the blockage ratio has been presented.
5. The tail shape coefficients of reasonably streamlined trains will normally be smaller than 1.0, implying a loss coefficient smaller than β_z^2.
6. Train drag is also influenced by tunnel resistance coefficients, albeit less strongly than by train coefficients. The greatest uncertainty in tunnel resistance is unsteady skin friction.
7. The scaling laws for the various coefficients are different. It is not possible to deduce a simple relationship between overall train drag and the train/tunnel blockage ratio.
8. There is a strong need for further measurements at full scale:
   (a) to assess the accuracy of the proposed methods of extrapolation and
   (b) to provide reference values from which to extrapolate data for specific trains in different tunnels.

REFERENCES

1 **Vardy, A. E.** and **Fox, J. A.** Compressible and leaky trains in tunnels. *Proc. Instn Mech. Engrs, Part D*, 1987, **201**(D3), 209–215.
2 **Schultz, M.** and **Sockel, H.** Pressure transients in short tunnels. Proceedings of Seventh International Symposium on *The aerodynamics and ventilation of vehicle tunnels* (Ed. A. Haerter), Brighton, 27–29 November 1991, pp. 221–237 (BHR Group, Cranfield).
3 **Miller, D. S.** *Internal flow systems*, 2nd edition, 1990 (BHR Group, Cranfield).
4 **Matsuo, K., Aoki, T., Kashimura, H., Iwamoto, K., Noguchi, Y.** and **Tsujimoto, Y.** Numerical simulation of an impulsive wave emitted from an exit of high-speed railway tunnel. Proceedings of Third International Conference on *Computer aided design, manufacture and operation in the railway and other advanced mass transit systems*, Washington, D.C., 18–20 August 1992, Vol. 2, pp. 455–463.
5 **Woods, W. A.** and **Pope, C. W.** Secondary aerodynamic effects in rail tunnels during vehicle entry. Proceedings of Second International Symposium on *The aerodynamics and ventilation of vehicle tunnels*, Cambridge, 23–25 March 1976, C56–C71 (BHR Group, Cranfield).
6 **Dayman, B., Hammitt, A. G., Holway, H. P., Tucker, C. E.** and **Vardy, A. E.** Alleviation of pressure pulse effects for trains entering tunnels. US Department of Transport report UMTA-MA-06-0100-79-10, 1979.
7 **Glöckle, H.** and **Pfretzschner, P.** High speed tests with ICE/V passing through tunnels. Proceedings of Sixth International Symposium on *The aerodynamics and ventilation of vehicle tunnels*, Durham, 27–29 September 1988, pp. 23–44 (BHR Group, Cranfield).
8 **Gaillard, M. A.** Aerodynamic measurements with high-speed trains (250 km/h) in the Heitersberg Tunnel. Proceedings of Third International Symposium on *The aerodynamics and ventilation of vehicle tunnels*, 19–21 March 1979, pp. 281–302 (BHR Group, Cranfield).
9 **Fox, J. A.** and **Henson, D. A.** The prediction of the magnitudes of pressure transients generated by a train entering a single tunnel. *Proc. Instn Civ. Engrs*, 1971, **49**(5), 53–69.
10 **Woods, W. A.** and **Pope, C. W.** A generalised flow prediction method for the unsteady flow generated by a train in a single track tunnel. Proceedings of International Symposium on *The aerodynamics of transportation*, Niagara, USA, 18–20 June 1979, pp. 137–151 (American Society of Mechanical Engineers, New York).
11 **Schlichting, H.** *Boundary layer theory*, 7th edition, 1979 (McGraw-Hill, New York).
12 **Jain, A. K.** Accurate explicit equation for friction factor. *J. Hydraul. Engng, ASCE*, 1976, **102**, 674–677.
13 **Brunone, B., Golia, U.** and **Greco, M.** Modelling of fast transients by numerical methods. Proceedings of Ninth Round Table IAHR Group, Valencia, Spain, 1991, pp. 273–280.
14 **Schultz, M.** and **Sockel, H.** The influence of unsteady friction on the propagation of pressure waves in tunnels. Proceedings of Seventh International Symposium on *The aerodynamics and ventilation of vehicle tunnels* (Ed. A. Haerter), Brighton, 27–29 November 1991, pp. 123–136 (BHR Group, Cranfield).
15 **Vardy, A. E.** Approximating unsteady friction at high Reynolds numbers. Proceedings of International Conference on *Unsteady flow and fluid transients*, Durham, 29 September–2 October 1992, pp. 21–29 (Balkema Press, Wallingford).
16 **Barrow, H.** and **Pope, C. W.** A simple analysis of flow and heat transfer in railway tunnels. *Heat and Fluid Flow*, 1987, **8**(2), 119–123.
17 **Hara, T.** Method of measuring the aerodynamic drag of trains. *Bull. J. Soc. Mech. Engrs*, 1965, **8**(31), 390–396.

18 Gawthorpe, R. G., Pope, C. W. and **Green, R. H.** Analysis of train drag in various configurations of long tunnel. Proceedings of Third International Symposium on *The aerodynamics and ventilation of vehicle tunnels*, Sheffield, 19–21 March 1979, pp. 257–280 (BHR Group, Cranfield).

19 Maeda, T., Kinoshita, M., Kajiyama, H. and **Tanemoto, K.** Estimation of aerodynamic drag of Shinkansen trains from pressure rise in tunnel. Proceedings of Sixth International Symposium on *The aerodynamics and ventilation of vehicle tunnels*, Durham, 27–29 September 1988, pp. 61–78 (BHR Group, Cranfield).

20 Gaillard, M. A. Aerodynamics of trains in tunnels. Proceedings of First International Symposium on *The aerodynamics and ventilation of vehicle tunnels*, Canterbury, 10–12 April 1973, pp. J33–J47 (BHRA Group, Cranfield).

21 Vardy, A. E. Aerodynamic drag on trains in tunnels. Part 1: synthesis and definitions. *Proc. Instn Mech. Engrs, Part F*, 1996, **210**(F1), 29–38.